Analysis of the properties of a dual-core plasmonic photonic crystal fiber polarization splitter

Abdul Khaleque[1] · Evgeny G. Mironov[1] · Haroldo T. Hattori[1]

Abstract In this work, the main properties of a dual-core plasmonic photonic crystal fiber that can split an incoming signal into two orthogonal polarization states are analyzed by using finite element method. The proposed splitter has a short length of 117 μm, being capable of splitting an incoming wave into two orthogonal states in the wavelength range between 1250 and 1710 nm. The main properties of the splitter are calculated such as extinction ratio, bandwidth, dispersion, mode-field-diameter and splice loss—the device would have a mode-field diameter around 4 μm and a splice loss below 5 dB.

1 Introduction

There are many physical phenomena nowadays that are polarization sensitive and need to be excited with the correct polarization state to be observed. In addition, the excitation of multiple polarization states can lead to distortion in optical communication systems, since different polarization states may travel at different speeds and arrive at different times in the receiver. A polarizer could be used to avoid the aforementioned problems and, in many cases, a fiber-based polarizer can be useful to directly select a certain polarization in existing optical fiber communication systems and distributed sensors. Early polarization splitters were fabricated in conventional fibers [1–3], resulting in long splitters (typically several millimeters long) with small bandwidth (a few nanometers linewidth).

Better polarizers and polarization splitters can be created by using photonic crystal fibers (PCFs) because of their desirable properties such as endless single-mode transmission [4], high nonlinearity [5], anomalous dispersion [6, 7] and high birefringence [8–10]. In addition, there are more parameters that can be controlled in PCFs: the diameters of holes, pitch and different materials can be added to holes (e.g., metals [11–15]). On the other hand, typical plasmonic devices are polarization sensitive and, by adding metals to the fiber, we can excite plasmonic waves [16–19] that are solely excited by certain polarization states—ideal property that can be used to create polarizers and polarization splitters. In metal filled or coated PCFs, when the fiber core modes and surface plasmon polariton (SPP) modes closely match, the energy in the core will strongly couple into the SPP modes around the metal wires for the specific mode. Metal wires have been successfully added to PCFs by different groups [20–22]—for example, Tyagi and co-workers [21] added a gold wire of diameter of 260 nm to a PCF. The advantage of exciting a plasmonic wave is that it generally leads to shorter splitter lengths and larger bandwidths when compared with conventional all-dielectric splitters [24–32].

Many of the reported results on PCFs with filling or selectively metal coating were based on a single core PCF. The advantage of adding another core to the structure is the possibility of creating a polarization splitter [14, 15, 23] which could be used, for example, in polarization multiplexing systems. However, it is challenging to produce at the same time, a compact and ultra-broadband splitter. Some broadband polarization splitters have been proposed in the literature [33–36], but they generally are long (close to 1 mm) and generally have linewidths of less than 100 nm.

✉ Abdul Khaleque
  abdul.khaleque@student.adfa.edu.au

[1] School of Engineering and Information Technology, University of New South Wales, Canberra, ACT 2610, Australia

In this paper, a compact gold-filled DC-PCF is proposed based on five air hole rings in a hexagonal lattice, being capable of splitting an incoming light into two orthogonal polarization states from 1250 to 1710 nm. The proposed 117-μm-long polarization splitter fiber with a bandwidth of 460 nm is a promising candidate for optical communication systems, covering many commercial communication bands (e.g., *O*, *E*, *S*, *C*, *L* and *U* bands).

2 Basic description of the device

The cross section of the DC-PCF that can split the incident light into two orthogonal polarization states is shown in Fig. 1a: it consists of a hexagonal lattice with 5 layers of air holes. The lattice constant of the structure is Λ and cores A and B are created by removing two air holes. Around cores A and B, four holes (as shown in Fig. 1a) are increased (holes with diameters d_1), while four other holes are decreased (with diameters d_2). The two central circular air holes in the structure are converted into elliptical air holes by changing the diameters of the air holes along the *y* direction with an ellipticity defined by $e = d_x/d_y$, where d_x and d_y are the major and minor axes diameters of the elliptical holes. Finally, two air holes along the vertical direction are selectively filled with gold wires (see Fig. 1a for details) with a diameter d_m (=d).

The background material is pure silica, and its material dispersion is given by Sellmeier's formula [37]. The relative permittivity of gold is given by an improved Drude–Lorentz model for metal [38] as,

$$\varepsilon_m = \varepsilon_\infty - \frac{\omega_D^2}{\omega(\omega - j\gamma_D)} - \frac{\Delta\varepsilon.\Omega_L^2}{(\omega^2 - \omega_L^2) - j\Gamma_L\omega} \quad (1)$$

where ε_m is the relative permittivity of the metal, ε_∞ is the relative high frequency permittivity, $\Delta\varepsilon$ is a weighting factor, ω is the angular frequency of the incident light, ω_D and γ_D are the plasma and damping frequencies, Ω_L and Γ_L represent the frequency and the spectral width of the Lorentz oscillator. Table 1 shows the parameters of the gold, which are in good agreement with the measured values at optical frequencies [38].

The basic analysis of the device follows the coupled mode theory proposed by Jiang and co-authors [36]. Initially, the modes in the DC-PCF can be described as a superimposition of even and odd modes as can be observed in Fig. 1b. In Fig. 1b, the arrows indicate the direction of the polarization, clearly showing the parity of even modes and the directions of the *x*-polarized and *y*-polarized modes. Similarly to Jiang [36], we define the coupling lengths for different polarization states as [29],
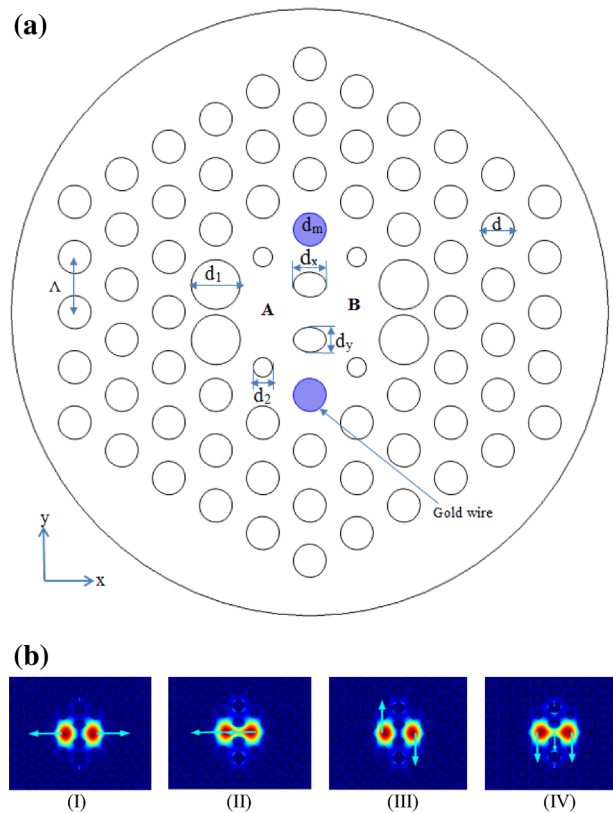

Fig. 1 a Cross section of the proposed gold-filled DC-PCF and **b** description of the electric field profile for the modes in the structure: (*I*) odd mode of *x*-polarization (*II*) even mode of *x*-polarization (*III*) odd mode of *y*-polarization (*IV*) even mode of *y*-polarization

Table 1 Values of the optimized parameters to fit the experimental data of bulk gold

ε_∞	$\omega_D/2\pi$ (THz)	$\gamma_D/2\pi$ (THz)	$\Omega_L/2\pi$ (THz)	$\Gamma_L/2\pi$ (THz)	$\Delta\varepsilon$
5.9673	2113.6	15.92	650.07	104.86	1.09

$$L_{x,y} = \frac{\lambda}{2\left(n_{x,y}^{\text{even}} - n_{x,y}^{\text{odd}}\right)} \quad (2)$$

where the superscripts refer to the even or odd mode, $L_{x,y}$ represents the coupling lengths for the *x*- and *y*-polarized directions, *n* and λ are the effective refractive index and free space wavelength, respectively. The two polarized states launched into one core can be separated whenever $mL_x = nL_y = L$, where *m* and *n* are positive integers with opposite polarity and *L* is the length of the splitter. The coupling length ratio (CLR) is defined as [36],

$$\text{CLR} = \frac{L_y}{L_x} \tag{3}$$

It is assumed that the input power P_{in} is pumped into core A, the output power (P_{out}) of core A in x- and y- polarized states can be calculated as [29],

$$P_{out}^{x,y} = P_{in} \cos^2\left(\frac{\pi L}{2L_{x,y}}\right) \tag{4}$$

Similarly, the output power (P_{out}) of core B in x- and y-polarized states can be calculated as [29],

$$P_{out}^{x,y} = P_{in} \sin^2\left(\frac{\pi L}{2L_{x,y}}\right) \tag{5}$$

Since the basic idea is to choose L such that all power for x-polarization remains in core A, while most of the y-polarization power is transferred to core B or vice versa, it is desirable to have CLR as either 2 ($L_y > L_x$) or 1/2 ($L_y < L_x$) [35]. Besides that, it is better to have relatively flat coupling lengths for the two polarization states to produce ultra-broadband splitter which will not be very sensitive to the wavelength, [35]. In this article, due to $L_y > L_x$, CLR = 2 is used to design the polarization splitter.

3 Simulation results and discussions

In order to investigate the characteristics of the proposed DC-PCF polarization splitter, full-vector finite element method (FEM-COMSOL Multiphysics) with perfectly matched layer (PML) boundary condition is used. The polarization properties are also investigated: the dispersion relation of second-order SPP modes and four supermodes are numerically calculated and shown in Fig. 2. It can be observed in Fig. 2 that the coupling is highly affected by the 2nd order SPP modes (these SPP modes have are similar to quadrupoles as seen in the inset): the phase matching condition takes place between the second-order SPP modes and core supermodes at the wavelength of 1020, 1060, 1070, and 1080 nm, respectively. To be more precise, several phase matching points of core supermodes are induced by the resonance of SPP supermodes: by adding more than one gold wire, discrete SPP modes interact with each other, creating plasmonic (SPP) supermodes and each supermode has a different phase constant at given wavelength [13]. In this case, x-even, y-even, y-odd, and x-odd core supermodes are phase matched (indicated by four points of a, b, c, d) with four individual 2nd SPP supermodes which are shown in the subplot of Fig. 2.

On the other hand, there is no coupling between the first-order *SPP* modes and the core supermodes due to their high effective refractive indices when compared with the core supermodes [11–15]—and hence they are omitted
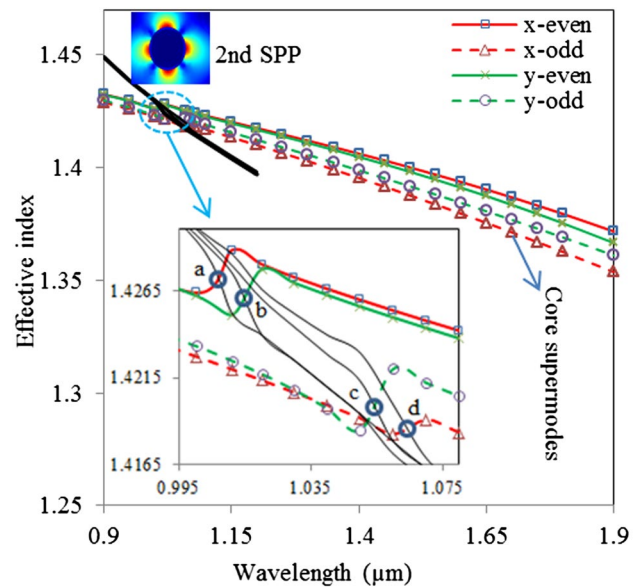

Fig. 2 Dispersion relation of the proposed gold-filled DC-PCF

in Fig. 2. Also, third- and higher-order SPP modes are not shown in Fig. 2 because of their weak coupling with core supermodes [12–14].

We have optimized all parameters (i.e. Λ, d, d_m, d_1, d_2, d_x, d_y) of the proposed structure to obtain an expected optimum CLR of 2. The optimized parameters for the proposed DC-PCF structure are found to be $\Lambda = 1.6$ μm, $d = d_m = 1.0$ μm, $d_1 = 1.5$ μm, $d_2 = 0.5$ μm, $d_x = 0.85$ μm, $d_y = 0.5$ μm, $e = 1.7$ and the CLR value is close to 2 under these optimized structural parameters.

According to the numerical results, the optimized values are $L_y = 117.0$ μm, $L_x = 58.51$ μm—leading to a CLR = 1.99966 at the wavelength of 1.55 μm. As can be observed in Fig. 3a, b, the addition of the gold wires allow CLR to reach values close to 2.0, what would not be possible in the absence of gold—the birefringence of the fibers without the gold wires cannot ever produce a CLR of 2.0.

More importantly, the coupling lengths of the two polarization states (L_x and L_y) are relatively flat (as shown in Fig. 3a) in the broad wavelength range between 1250 and 1710 nm, producing a broadband polarization splitter. Therefore, after assessing the results shown in Fig. 3a, b, it is necessary to couple light into a plasmonic mode to produce a compact polarization splitter.

Figure 4a shows the normalized output power variations in core A of the two polarization states versus the propagation distance at the wavelength of 1.55 μm. The splitter length is indicated by a dashed line, and it is assumed that the incident light enters through core A, the normalized power difference between x- and y-polarized light reaches the highest value at a propagation distance of 117 μm,
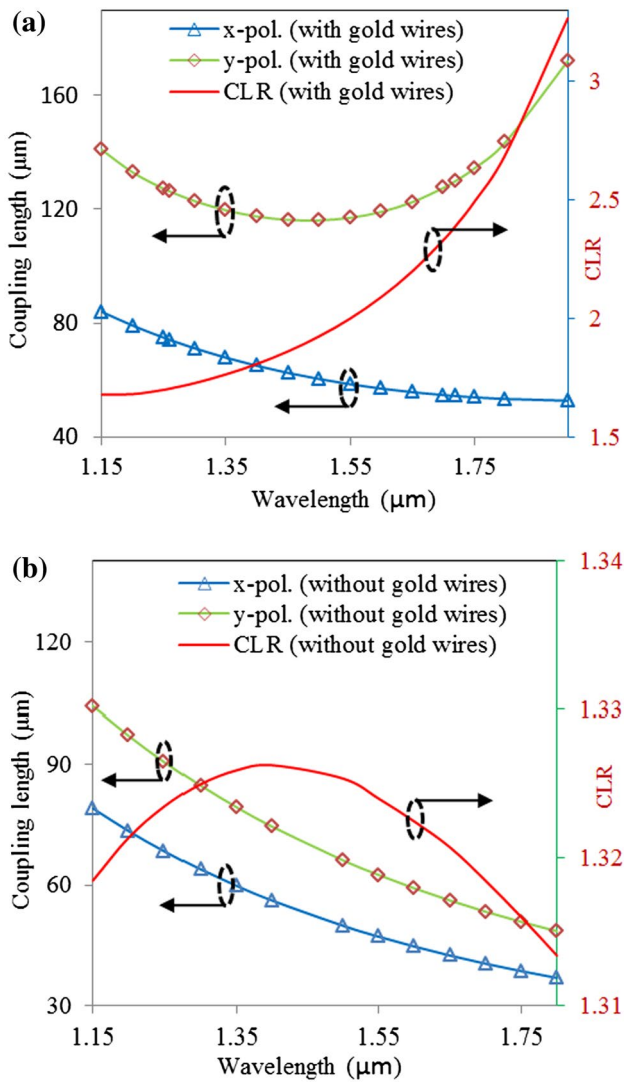
Fig. 3 CL and CLR versus wavelength of the proposed DC-PCF structure **a** with gold wires; **b** without gold wires for optimal geometrical parameters

Fig. 4 a The normalized output power variation along the propagation distance in core A; **b** Extinction ratio (ER) spectra at the optimal geometrical parameters

meaning that *x*-polarized output power reaches its maximum, while the *y*-polarized output power is close to zero at the length of 117 μm. The situation is reversed in core B (not shown): *y*-polarized output power will reach its maximum value while the *x*-polarized output power will be close to zero at the length of 117 μm. Hence, the incident light, which includes *x*- and *y*-polarized states, is separated into *x*-polarized light at core A and *y*-polarized light at core B by the device. In addition, the output power is attenuated due to the ohmic losses of the metallic wires and the leaky core structure in the *y*-direction.

In Fig. 4a, it can also be noted that the power decreases with the distance as is expected with the addition of gold: gold introduces ohmic losses to the structure whereby part of the power is dissipated through heat generation. In
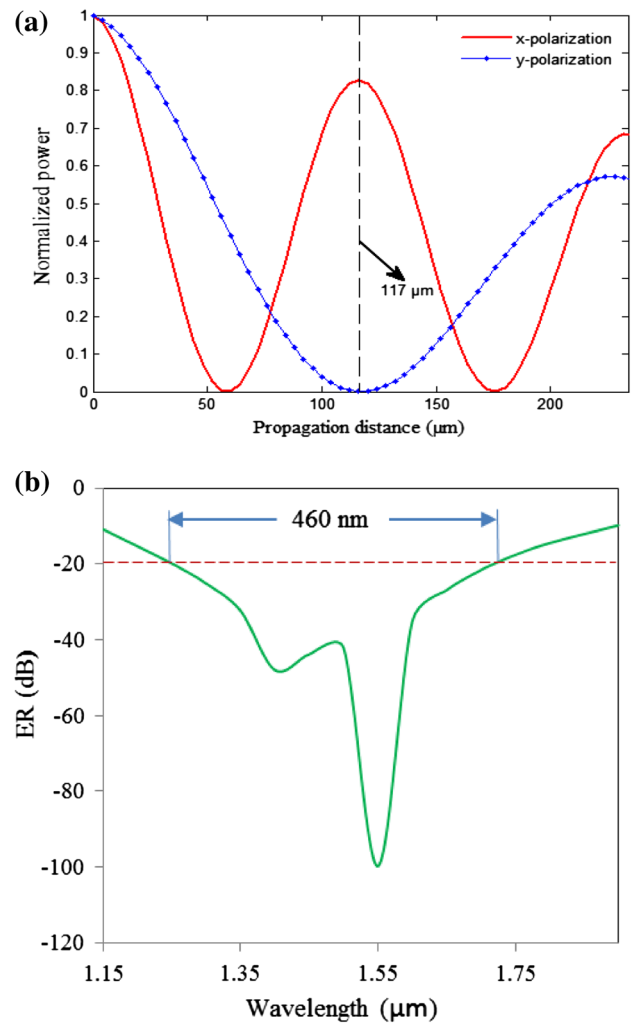
addition, the confinement in the fiber cores is never perfect and radiation losses may also lead to a reduction in the total power. Other sources of potential losses include splice loss, insertion loss, scattering loss and eventually microbending and bending losses.

The crosstalk between the different polarization states can be assessed by the Polarization extinction ratio (ER), which is defined as the power of a particular polarization in the expected output core compared to the power of the other polarization in the same core. Due to the use of two identical symmetrical cores A and B in our proposed structure, the ERs in the two cores are the same. Hence, we evaluate the ER only in core A which can be defined as [36],

$$ER = 10 \log \left(\frac{P_{out}^y}{P_{out}^x} \right) \qquad (6)$$

Figure 4b shows the variation of ER for core A as a function of wavelength when the splitter length is 117 μm. It is clear from Fig. 4b that a very high extinction ratio of −100 dB is achieved at the wavelength of 1.55 μm. More importantly, an ER better than −20 dB is obtained over a large bandwidth of 460 nm, from 1250 to 1710 nm, covering two communication bands.

3.1 Influence of fiber parameters on the performance of the proposed splitter and feasibility of the design

In a standard fiber draw, ±1 % variations in fiber global diameters may occur [39] during the fabrication process. To account for structural variations, all the designed parameters are varied to assess the potential fabrication of the device. In this section, the effects of different geometrical parameters on ER over the expected wavelength ranges are calculated and discussed. We follow a similar procedure employed by Lu and co-workers [35], where we calculate the influence of different parameters on the optimized design.

Figure 5a shows ER versus wavelength for different values of lattice constant: Λ is increased from 1.5 to 1.65 μm, while other parameters are fixed. The initial effect of changing Λ is the weakening of the matching of the fiber modes with the 2nd plasmonic mode, leading to weaker 'dips' in ER. Secondly, the wavelength at which CLR = 2.0 also changes since the mode field profiles also change when cores A and B areas change with ER. Due to an increase of the lattice constant to 1.65 μm, peak ER value
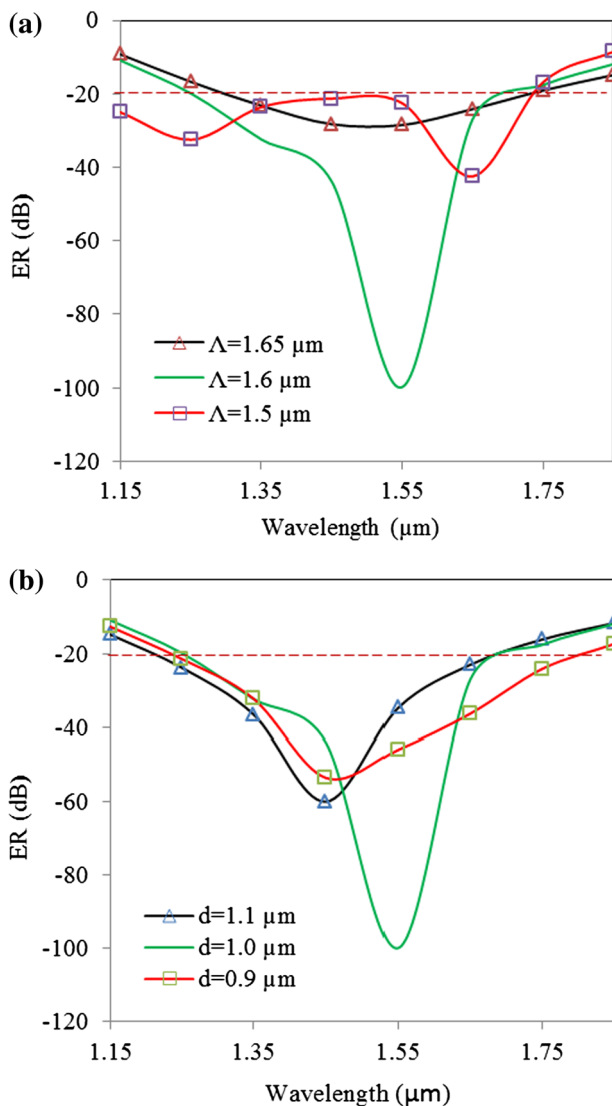

Fig. 5 Effect of **a** lattice constant Λ, and **b** diameter d on the ER spectra of the proposed DC-PCF
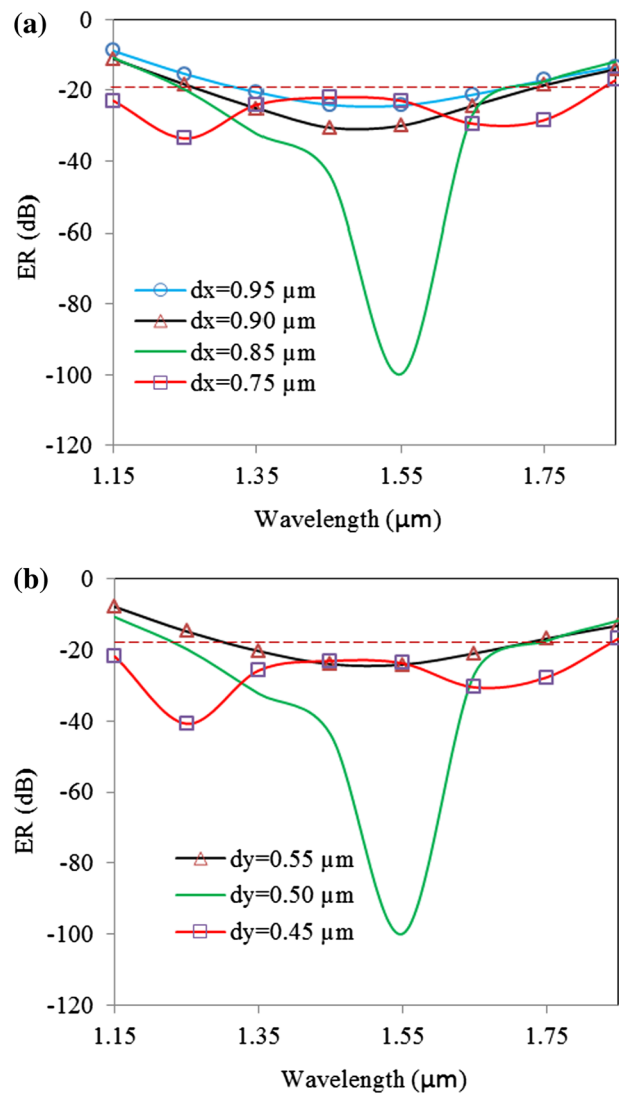
Fig. 6 Effect of the diameters of the elliptical holes **a** d_x, and **b** d_y on the ER spectra of the proposed DC-PCF

at 1.55 μm changes from −100 to −30 dB but the working region remains the same, i.e., from 1260 to 1720 nm, with a slightly shift to lower wavelengths. However, the bandwidth (<−20 dB) is increased to 640 nm, from 1110 to 1740 nm, when Λ decreased by around 7 % to 1.5 μm (as shown in Fig. 5a).

On the other hand, the variation of d (about 10 %) does not considerably degrade the performance of the fiber: the working bandwidth becomes broader (1240–1800 nm) and 500 nm (1220–1720 nm) as d is changed to 0.9 and 1.1 μm, respectively, as shown in Fig. 5b. In addition, a small wavelength shift of the dip of the ER is also observed in Fig. 5b. A change in the diameter (d) does not significantly change the effective refractive indices of the x- and y-polarized modes and, therefore, they only produce a small change in their coupling lengths with the wavelengths—the net result is a small variation of ER with small changes in the diameter. Intuitively, a small change in d will not greatly affect the distribution of the core modes and therefore their properties will not be affected much, as long as the cladding is in its photonic bandgap region.

Therefore, as aforementioned earlier, CLR is close to 2.0 at the wavelength of 1.55 μm because the fiber structure is optimized at this wavelength; hence, the value of the ER dip will change with variations of Λ and d (same for other parameters variation), but it is still below −20 dB—moreover there is no significant changes in the bandwidth of the splitter.

Figure 6 shows the effect of changing the major axis (d_x) and minor axis (d_y) of the center elliptical air holes on ER spectra: d_x changed from 0.95 to 0.75 μm while d_y changed from 0.55 to 0.45 μm, while the optimized parameters remained the same. According to Fig. 6a, ER is lower than −20 dB in the wavelength range between 1265 and 1740 nm as d_x increased (by 5.5 %) to 0.9 μm and then slightly decreased to 400 nm as d_x increased to 0.95 μm (about 11 %).

On the other hand, ER (<−20 dB) bandwidth is increased to 700 nm as d_x decreased to 0.75 μm, as can be observed in Fig. 6a. Also, the effect of the change of d_y by about 10 % is shown in Fig. 6b: the bandwidth is broadened to 660 nm when d_y is decreased to 0.45 μm, while the bandwidth is reduced to 440 nm as d_y increased to 0.55 μm (over 9 %). Based on the results presented in Fig. 6a, b, we can conclude that the proposed structure can still work on a broad bandwidth (<−20 dB) in spite of variations of d_x and d_y by more than ±5 %. A change in d_x and/or d_y leads to a change in the ellipticity of the air holes and therefore change the birefringence of the whole structure—making the holes more circular generally leads to higher (weaker) values of ER, that can be observed in the plots.

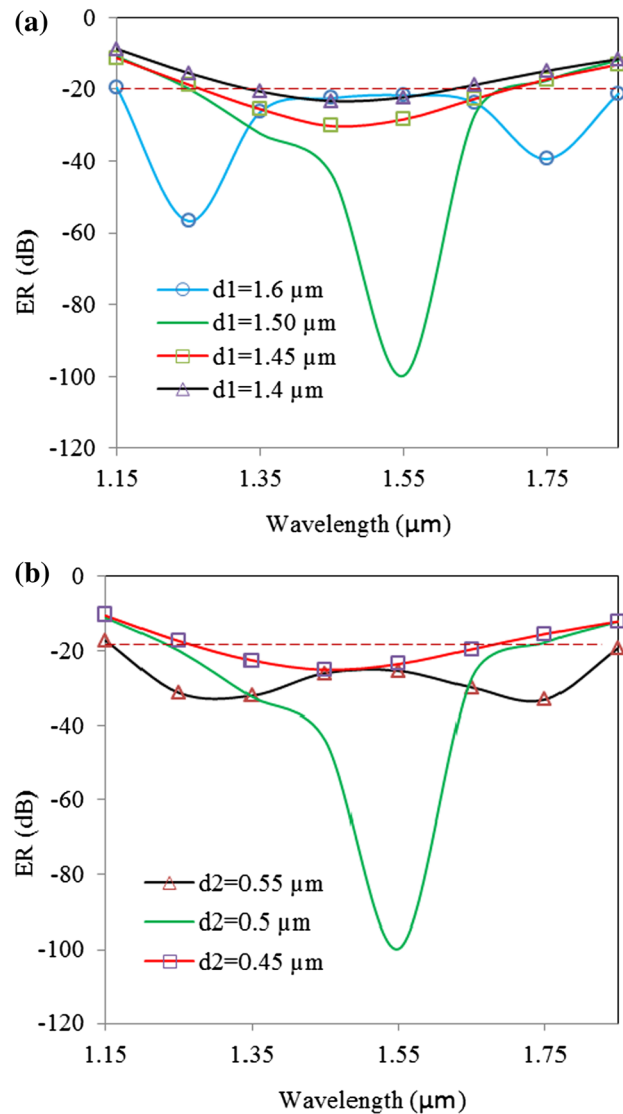Figure 7a, b show the effect of changing diameters d_1 and d_2 on the ER spectra. It is shown in Fig. 7a that the

Fig. 7 Effect of the diameters **a** d_1, and **b** d_2 on the ER spectra of the proposed DC-PCF

bandwidth remains the same as d_1 is decreased to 1.45 μm, but the bandwidth increases to 710 nm, as d_1 increases to 1.60 μm. The worst performance is observed when d_1 is decreased to 1.40 μm (about 7 %) when the bandwidth is reduced to 370 nm. On the other hand, a similar behavior in term of bandwidth is observed when d_2 is changed (nearly 10 %) from 0.55 to 0.45 μm: the bandwidth changes to 700 and 420 nm, as d_2 increased and decreased to 0.55 and 0.45 μm, respectively, as is shown in Fig. 7b. Hence, the proposed fiber maintains good performance over the reasonable variation of both d_1 and d_2.

An explanation for this behavior can be extracted from Fig. 8a–c although a change in d_1 weakens the matching between the 2nd plasmonic mode and both x- and y-polarized modes (y-polarized mode has more effect than
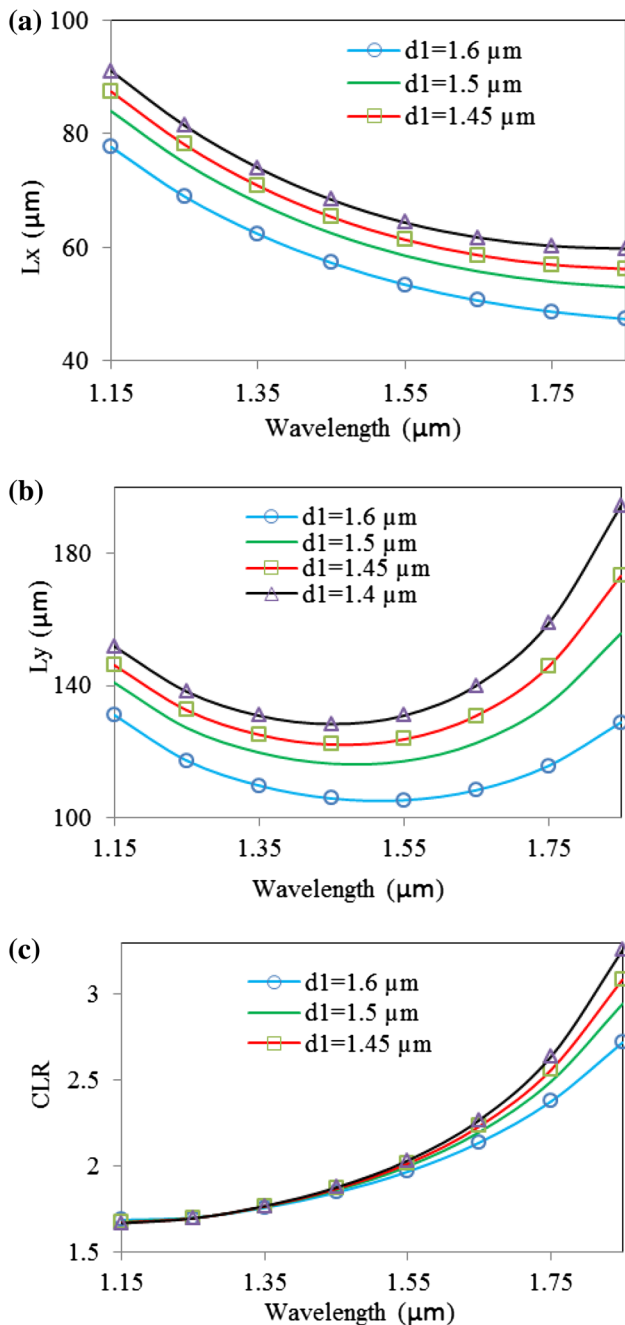
Fig. 9 Effect of the gold filled diameters, d_m variation on the ER spectra of the proposed DC-PCF

Fig. 8 Effect of changing d_1 on coupling lengths (x- and y-polarized) and coupling length ratio **a** L_x, **b** L_y, **c** *CLR*

The effects of variations of the gold filled diameters (d_m) on ER are shown in Fig. 9, in which d_m is varied from 1.1 to 0.9 μm. The range of operation of the fiber splitter (ER < −20 dB) increases with a 10 % reduction of d_m, i.e., bandwidth becomes broader to 660 nm. On the other hand, the working bandwidth does not significantly change when d_m is increased to 1.05 μm (nearly 5 %), and then slightly decreases to 440 nm as d_m is increased to 1.1 μm (nearly 10 %). In this case of $d_m = 1.1$ μm, the effect of the increase of d_m is negligible for x-polarized mode but y-polarized mode is much more affected: y-polarized coupling length is increased at the longer and shorter wavelength regions, hence making it harder to get appropriate CLR. Therefore, the proposed fiber can still work with expected performance for more than ±5 % variations in d_m.

The variations of different parameters show that an actual fabrication of the device is feasible although it is difficult to fabricate such complex device with different hole diameters and metal inclusions. By now, there are different techniques [20–22, 44–46] available to produce the DC-PCF structure, such as femtosecond laser microscanning [46] or novel splicing-based pressure assisted melt-filling technique [22] proposed by Russel and colleagues, for creating metallic nanowires in a hollow channel in microstructured silica fibers—wires with diameters as small as 120 nm have been created at a filling pressure of 300 bar. As previously mentioned, Tyagi and co-workers have used a direct fiber drawing technique [21] to produce high-quality gold wires, and a selective hole closure technique [20] was employed to fill with Ge some air holes—molten material at high pressure was inserted at specific holes in this case. Moreover, Lee and colleagues [44] analyzed a

x-polarized mode), it does not significantly affect CLR for small variations of d_1, therefore remaining close to 2.0, meaning that the bandwidth is not significantly changed with d_1 (or with similar arguments to d_2). In addition, it can be seen from Fig. 8a–c that rate of change of these matching between plasmonic and fiber modes is higher in longer wavelength regions, resulting in more significant bandwidth reduction for longer wavelengths.
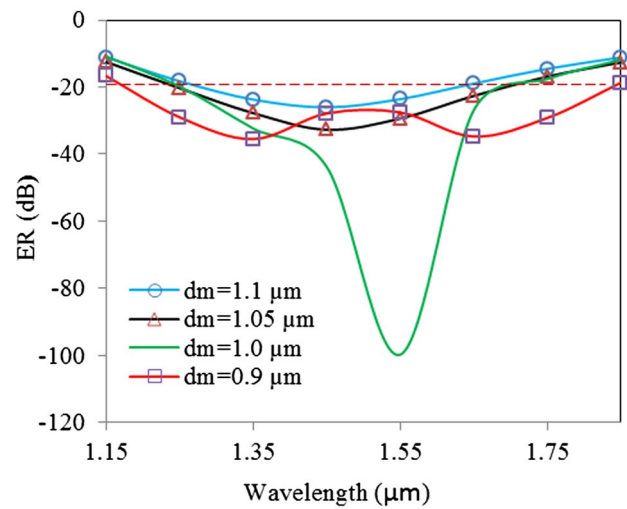
coupling between surface plasmon mode to nanowires, while Schmidt et al. [45] fabricated gold and silver nanowires in a triangular lattice with diameter down to 500 nm. In addition, microstructure optical fibers with uniformly oriented elliptical holes have been fabricated by Issa et al. [47]: a simple technique that relies on hole deformation during fiber draw was used to achieve a high degree of hole ellipticity. With constant evolution of fabrication technology, it might be possible to fabricate the proposed structure in future.

3.2 Calculation of propagation properties of the proposed DC-PCF

Additional parameters of the proposed DC-PCF are calculated: the chromatic dispersion, mode field diameter (MFD) and splice loss. The chromatic dispersion D is calculated by [40],

$$D = -\frac{\lambda}{c} \frac{d^2 Re[n_{\text{eff}}]}{d\lambda^2} \qquad (7)$$

where, $Re[n_{\text{eff}}]$ is the real part of n_{eff}, λ is the wavelength and c is the velocity of light in vacuum. The material dispersion given by Sellmeier formula is directly included in the calculation.

Figure 10 shows the wavelength dependence of x- and y-polarized dispersions under the optimized structural parameters and fiber's global diameter variation of order ±5 % around the optimum value. It is shown in Fig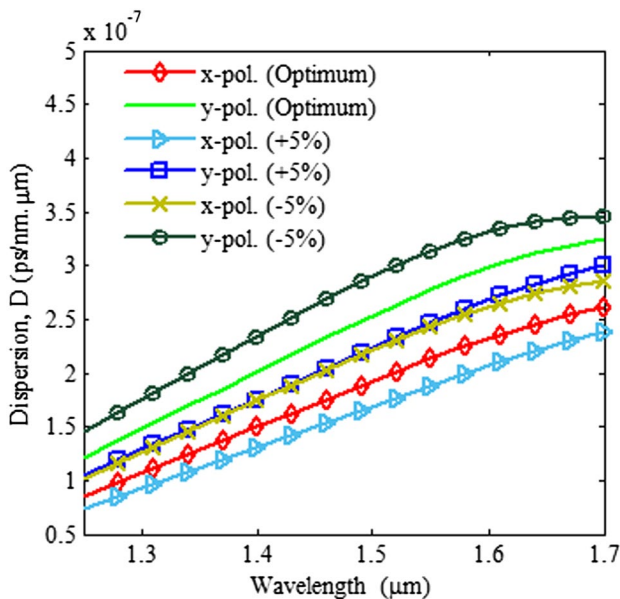. 10 that y-polarized dispersion is slightly higher than the x-polarized dispersion due to the leaky core structure in the y-direction. Also, dispersions increase with the wavelength: dispersion increased from 0.8×10^{-7} to 2.7×10^{-7} ps/nm μm and 1.25×10^{-7} to 3.25×10^{-7} ps/nm μm, respectively, for the x- and y-polarized states when the free-space wavelength changes from 1250 to 1700 nm. The dispersion properties show opposite trend with ±5 % variations of fiber's global diameter: dispersion for both x- and y-polarized states slightly decrease and increase around the optimum value, respectively, as shown in Fig. 10.
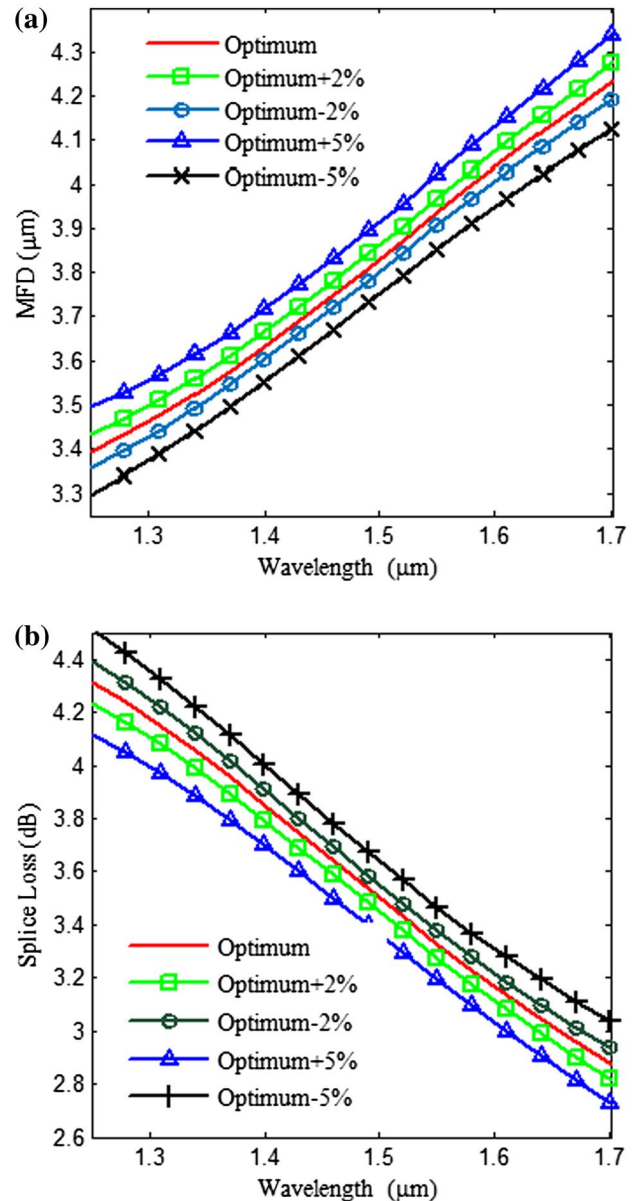

Fig. 11 a Mode field diameter (MFD) and b Splice losses of the proposed DC-PCF for optimum design parameters and also for fiber's global diameter variation of order ±2 to ±5 % around the optimum value

Fig. 10 Dispersion properties of the proposed DC-PCF for fiber's global diameter (Λ, d, d_m, d_1, d_2, d_x, d_y) variation of order ±5 % around the optimum value

Confinement losses (Lc) and effective areas (A_{eff}) can be calculated by using the following formulae [40],

$$Lc = 8.686 \times Im[k_0 n_{eff}] \times 10^3 dB/km \qquad (8)$$

$$A_{eff} = \left(\int\limits_{-\infty}^{\infty} \int\limits_{-\infty}^{\infty} |E|^2 dxdy \right)^2 \bigg/ \left(\int\limits_{-\infty}^{\infty} \int\limits_{-\infty}^{\infty} |E|^4 dxdy \right) \qquad (9)$$

where, E is the electric field derived by solving Maxwell's equations and λ is the free-space wavelength.

The confinement losses for x- and y-polarized states are different for different wavelengths: loss increases with the increase of the wavelength. Under the optimized designed parameters, the corresponding losses for x- and y-polarized states are 0.375 and 0.497 dB at 1.25 µm, 0.46 and 0.632 dB at 1.35 µm, 0.619 and 0.86 dB at 1.45 µm, 0.844 and 1.165 dB at 1.55 µm, 1.11 and 1.53 dB at 1.65 µm, 1.26 and 1.72 dB at 1.70 µm of wavelength, respectively, for a splitter length of 117 µm.

Figure 11a, b show the mode field diameter (MFD) and the splice loss between the proposed DC-PCF and a conventional single-mode fiber (SMF). The MFD of the SMF is assumed to be 10.0 µm. The MFD of the proposed structure is calculated by the well-known Petermann II formula [41], and the splice loss is calculated by [42]

$$L_s = -20 \log_{10} \frac{2 w_{SMF} w_{PCF}}{w_{SMF}^2 + w_{PCF}^2} \qquad (10)$$

where, w_{SMF} and w_{PCF} are the MFDs of the SMF and proposed PCF-splitter, respectively.

The MFD and Splice loss in the wavelength range between 1250 and 1700 nm are shown in Fig. 11a, b: MFD increases from 3.40 to 4.21 µm and splice loss decreases from 4.3 to 2.8 dB. MFD and splice loss are 3.9 µm and 3.3 dB, respectively, at the wavelength of 1.55 µm for the optimized designed parameters. If the fiber's global diameters are changed up to ±5 %, there are no significant variations in those parameters. Because of the smaller MFD of the proposed fiber splitter, splice loss are high—but this would also be expected for highly nonlinear PCFs, and this high splicing loss could be eliminated by the use of recent splice free interconnection technique between SMFs and PCFs [43].

In terms of splicing, extra polarization maintaining fibers can be added at the end of the polarization splitter in either side of this 117 µm fiber during the fabrication of the device: additional polarization maintaining fibers can carry different polarizations to their final destinations (e.g., photodetectors) and could eventually be spliced with other fibers. Besides that, according to the Saval and co-workers [43] results, it is also possible to interconnect two fibers without splicing and the additional fibers would carry the signals with different polarization states.

Table 2 Comparison between properties of the proposed DC-PCF splitter and other splitter design

PCFs	Device length	Bandwidth (nm)	Working spectral region (nm)
Ref. [14]	0.6 mm	100 nm (<−20 dB)	1260–1360
Ref. [23]	0.782 nm	65 nm (<−20 dB)	1500–1565
Ref. [24]	5 mm	N/A	1550
Ref. [25]	1.7 mm	40 nm (<−11 dB)	1525–1565
Ref. [26]	1.9 mm	37 nm (<−20 dB)	1536–1573
Ref. [27]	2.592 mm	29 nm (<−15 dB)	1538–1567
Ref. [28]	9.08 mm	5.5 nm (<−20 dB)	1298–1303.5
Ref. [29]	15.4 mm	5 nm (<−20 dB)	1297–1302
Ref. [30]	10.69 mm	25.4 nm (<−20 dB)	1539–1564.4
Ref. [31]	8.7983 mm	20 nm (<−20 dB)	1540–1560
Ref. [32]	0.638 mm	N/A	1550
Ref. [33]	0.995 mm	80 nm (<−20 dB)	1500–1580
Ref. [34]	20 mm	90 nm (<−20 dB)	1450–1540
Ref. [35]	72 mm	400 nm (<−20 dB)	1230–1630
Ref. [36]	119.1 µm	249 nm (<−20 dB)	1417–1666
Prop. DC-PCF	117.0 µm	460 nm (<−20 dB)	1250–1710

A comparison is made between properties of the proposed DC-PCF fiber and other fibers designed for polarization splitter applications over the communication wavelength ranges. Table 2 compares those fibers according to the splitter length, working bandwidth and working wavelength regions. It is standard to expect ER better than −20 dB within the expected bandwidth region, meaning that the structure can work well within this wavelength range but structure can still work with ER slightly worse than −20 dB as shown in two splitters [25, 27] describes their working bandwidth <−11 and <−15 dB, respectively. According to Table 2, most of splitter lengths are in mm range with limited bandwidth and covering a part of communication wavelength range. For example, PCF in [35] proposed broad bandwidth of 400 nm but device length is 72 mm, while Ref. [36] presents compact length of 119.1 µm but bandwidth reduced to 249 nm. Therefore, it can be concluded that our proposed device of 117 µm in length is compact as well as can work in broad wavelength ranges (460 nm), covering all communication wavelength region.

4 Conclusions

To summarize, a compact DC-PCF selectively filled with gold wires is proposed showed ultra-broadband polarization splitting characteristics and its performance is numerically investigated by FEM. In addition, two gold wires have been added selectively to fill two holes in the fiber to produce compact length with high performance polarization splitter. Under the optimized value of the structural parameters, a compact length, high extinction ratio and ultra-broad bandwidth is achieved for the proposed polarization splitter fiber. The numerical results demonstrate that the polarization splitter has a very short length of 117 μm with the high extinction ratio of -100 dB at the wavelength of 1.55 μm. More importantly, this polarization splitter shows an ultra-broadband bandwidth of 460 nm, from 1250 to 1710 nm, with the extinction ratio better that −20 dB. This compact fiber could be useful as an ultra-broadband polarization splitter in broadband communication systems which could cover all communication bands (*O*, *E*, *S*, *C*, *L* and *U* bands). In addition to that, this study can also be used to produce other plasmonics-based optical devices.

References

1. A.N. Miliou, R. Srivastava, R.V. Ramaswamy, J. Lightwave Tech. **11**, 220 (1993)
2. C.W. Wu, T.L. Wu, H.C. Chang, IEEE Phot. Tech. Lett. **7**, 786 (1995)
3. G.D. Peng, T. Tjugiarto, P.L. Chu, Electron. Lett. **26**, 682 (1990)
4. J.C. Knight, T.A. Birks, R.F. Cregan, P.S.J. Russell, J.P. De Sandro, Elect. Lett. **34**, 1347 (1998)
5. N.G.R. Broderick, T.M. Monro, P.J. Bennett, D.J. Richardson, Opt. Lett. **24**, 1395 (1999)
6. S. Kim, C.S. Kee, Opt. Express **17**, 15885 (2009)
7. T. Fujisawa, K. Saitoh, K. Wada, M. Koshiba, Opt. Express **14**, 893 (2006)
8. M.J. Steel, R.M. Osgood Jr, J. Lightwave Tech. **19**, 495 (2001)
9. K. Suzuki, H. Kubota, S. Kawanishi, M. Tanaka, M. Fujita, Opt. Express **9**, 676 (2001)
10. T.P. Hansen, J. Broeng, S.E. Libori, E. Knudsen, A. Bjarklev, J.R. Jensen, H. Simonsen, IEEE Phot. Tech. Lett. **13**, 588 (2001)
11. Y. Du, S.G. Li, S. Liu, X.P. Zhu, X.X. Zhang, Appl. Phys. B **109**, 65 (2012)
12. A. Khaleque, H.T. Hattori, Appl. Opt. **54**, 2543 (2015)
13. A. Nagasaki, K. Saitoh, M. Koshiba, Opt. Express **19**, 3799 (2011)
14. P. Li, J. Zhao, Opt. Express **21**, 5232 (2013)
15. S. Zhang, X. Yu, Y. Zhang, P. Shum, Y. Zhang, L. Xia, D. Liu, IEEE Phot. J. **4**, 1178 (2012)
16. B. Shuai, L. Xia, Y. Zhang, D. Liu, Opt. Express **20**, 5974 (2012)
17. S. Zhang, K. Bao, N.J. Halas, H. Xu, P. Nordlander, Nano Lett. **11**, 1657 (2011)
18. H. Jiang, K. Xie, Y. Wang, Elect. Lett. **44**, 796 (2008)
19. X. Shan, U. Patel, S. Wang, R. Iglesias, N. Tao, Science **327**, 1363 (2010)
20. H.K. Tyagi, M.A. Schmidt, L. Prill Sempere, S. Russell, Opt. Express **16**, 17227 (2008)
21. H.K. Tyagi, H.W. Lee, P. Uebel, M.A. Schmidt, N. Joly, M. Scharrer, P.S.J. Russell, Opt. Lett. **35**, 2573 (2010)
22. H.W. Lee, M.A. Schmidt, R.F. Russell, N.Y. Joly, H.K. Tyagi, P. Uebel, P.S.J. Russell, Opt. Express **19**, 12180 (2011)
23. H. Chen, S. Li, G. An, J. Li, Z. Fan, Y. Han, Plasmonics **10**, 57 (2015)
24. L. Zhang, C. Yang, C. Yu, T. Luo, A.E. Willner, J. Lightwave Tech. **23**, 3558 (2005)
25. L. Zhang, C. Yang, Opt. Express **11**, 1015 (2003)
26. K. Saitoh, Y. Sato, M. Koshiba, Opt. Express **12**, 3940 (2004)
27. H. Chen, S. Li, T. Cheng, J. Modern Opt. **61**, 1696 (2014)
28. N.J. Florous, K. Saitoh, M. Koshiba, IEEE Phot. Tech. Lett. **18**, 1231 (2006)
29. N. Florous, K. Saitoh, M. Koshiba, Opt. Express **13**, 7365 (2005)
30. M.Y. Chen, J. Zhou, J. Lightwave Tech. **24**, 5082 (2006)
31. S. Liu, S.G. Li, G.B. Yin, R.P. Feng, X.Y. Wang, Opt. Comm. **285**, 1097 (2012)
32. Z. Zhang, Y. Tsuji, M. Eguchi, IEEE Phot. Tech. Lett. **26**, 541 (2014)
33. L. Zhang, C. Yang, IEEE Phot. Tech. Lett. **16**, 1670 (2004)
34. L. Rosa, F. Poli, M. Foroni, A. Cucinotta, S. Selleri, Opt. Lett. **31**, 441 (2006)
35. W. Lu, S. Lou, X. Wang, L. Wang, R. Feng, Appl. Opt. **52**, 449 (2013)
36. H. Jiang, E. Wang, J. Zhang, L. Hu, Q. Mao, Q. Li, K. Xie, Opt. Express **22**, 30461 (2014)
37. G.P. Agrawal, *Nonlinear Fiber Optics* (Academic press, New York, 2007)
38. A. Vial, A.S. Grimault, D. Macias, D. Barchiesi, M.L. de La Chapelle, Phys. Rev. B **71**, 085416 (2005)
39. W.H. Reeves, J.C. Knight, P.S.J. Russell, P. Roberts, Opt. Express **10**, 609 (2002)
40. K. Saitoh, M. Koshiba, T. Hasegawa, E. Sasaoka, Opt. Express **11**, 843 (2003)
41. K. Petermann, Elect. Lett. **19**, 712 (1983)
42. S.M. Razzak, Y. Namihira, J. Lightwave Tech. **26**, 1909 (2008)
43. S.G. Leon-Saval, T.A. Birks, N.Y. Joly, A.K. George, W.J. Wadsworth, G. Kakarantzas, P.S.J. Russell, Opt. Lett. **30**, 1629 (2005)
44. H.W. Lee, M.A. Schmidt, H.K. Tyagi, L.P. Sempere, P.S.J. Russell, Appl. Phys. Lett. **93**, 111102 (2008)
45. M.A. Schmidt, L.P. Sempere, H.K. Tyagi, C.G. Poulton, P.S.J. Russell, Phys. Rev. B **77**, 033417 (2008)
46. Y. Wang, C.R. Liao, D.N. Wang, Opt. Express **18**, 18056 (2010)
47. N.A. Issa, M.A. van Eijkelenborg, M. Fellew, F. Cox, G. Henry, M.C. Large, Opt. Lett. **29**, 1336 (2004)